Cooper Union for the Advancement of Science and Art

ChE 441 Final Project

Mathematical Modeling of the Effects of Liver Tumor Ablation on Temperature, Blood Flow, and Oxygen Transport

Author:
Joshua Mayourian

Instructor:
Professor Lepek

May 7, 2014

Abstract

Radiofrequency ablation is typically used to heat up malignant liver tissue to critical temperatures in order to kill cancerous cells. However, this hyperthermic process also has noticeable effects on the microvasculature of tumor tissue (i.e. capillary blood vessels). Specifically, it has been empirically shown that heating up cancerous tissue also affects blood flow and oxygen transport. Mathematical modeling is a powerful tool to analyze and control blood flow and oxygenation as a function of transient temperature rise within tissue. Therefore, in this study, a mathematical model was developed via COMSOL Multiphysics to describe the effects of radiofrequency ablation on blood flow and oxygen transport within tumor tissue. It was determined that the application of radiofrequency ablation on cancerous liver tissue for 60 seconds increases the average temperature of the tumor tissue from 37°C to 43°C. The hyperthermic effects of radiofrequency ablation subsequently resulted in an increase of capillary blood vessel radius by 30%, an increase in blood flow velocity by 70%, and an increase in overall oxygenation. This study shows that radiofrequency ablation can potentially be coupled with chemotherapy to enhance the efficacy of delivering pharmacological agents.

Table of Contents

List of Figures

List of Tables

Symbols

In order of appearance:

V	Electric Potential	V
ρ_f	Free-Charge Density	C/m^3
ϵ	Permittivity	Unitless
r	Radius	m
ϕ	Angular Coordinate	$^\circ$
z	Height	m
k	Thermal Conductivity	W/m/k
ρ	Density	kg/m^3
C_p	Specific Heat	J/kg/K
T	Temperature	K
Q	Joule Heating	W
σ	Electrical Conductivity	S
Q_m	Metabolic Heat Generation	W
Q_b	Blood Perfusion Heat Generation	W
ω_b	Blood Perfusion Coefficient	1/s

$\mathbf{u}$	Velocity vector	m/s
μ	Blood Viscosity	Pa·s
r_0	Initial Capillary Radius	m
T_0	Initial Temperature	K
P_{O_2}	Oxygen Partial Pressure	mm Hg
D	Diffusivity constant	m^2/s
M	Rate of metabolism	cm^3 O_2 cm^{-3}
a	Oxygen Solubility	cm^3 O_2 cm^{-3}/mm Hg

Introduction

Liver tumors are abnormal masses of liver tissue that grow at an uncontrollable rate [1, 2]. Tumors are classified into two groups by their ability to invade and damage nearby tissues [2] — cancerous (malignant) tumors are capable of invading surrounding tissues, while non-cancerous (benign) tumors are not [1, 2]. Malignant tumors are of special interest, as it is expected that nearly 23,000 people will die of liver cancer in 2014 alone [3]. Typical treatments for malignant tumors include surgery, radiotherapy, chemotherapy, liver transplantation, and radiofrequency ablation. The most common method for small tumors, radiofrequency ablation, is of interest in this study.

1.1 Radiofrequency Ablation

Radiofrequency ablation is the use of electromagnetic energy to heat up malignant tissue to critical temperatures in order to kill cancerous cells. This method is popular for its efficacy, controllability, minimal invasiveness, and low cost [4]. The high energy treatment is typically applied within tissue for approximately 60 seconds. It has been empirically shown that heating the tumor also has noticeable effects on the microvasculature of the tumor tissue (i.e. capillary blood vessels), by affecting blood flow and oxygen transport.

1.2 Hyperthermia Effects on Blood Flow and Oxygen Transport

Animal model studies have shown that blood flow and oxygen transport are positively affected during hyperthermia. For example, Endrich *et al* showed that heating an amelanotic melanoma of a hamster resulted in an increased blood flow in tumor microvasculature [5]. Furthermore, Shakil *et al* showed that hyperthermia results in increased tumor oxygenation (i.e. increased partial pressure of oxygen) [6]. This effect of hyperthermia on vasculature is extremely valuable, as controlling the blood flow and oxygenation can improve treatment efficacy. Specifically, controlling blood flow aids in delivery of pharmacological agents during chemotherapy [7]. Therefore, researchers find it worthwhile and valuable to computationally determine the effects of hyperthermia on blood flow and oxygen transport.

1.3 Objectives of this Study

Mathematical modeling is a powerful tool to analyze and control blood flow and oxygenation as a function of transient temperature rise within tissue. Therefore, in this study, a mathematical model was developed to describe the effects of radiofrequency ablation on blood flow and oxygen transport within tumor tissue. To mathematically describe the effects of radiofrequency ablation on blood flow and oxygen transport within tumor, COMSOL Multiphysics was used. The following general steps were taken in this study:

1. Develop the electric potential field profile due to radiofrequency ablation.

2. Develop the transient temperature profile due to radiofrequency ablation.

3. Determine the blood flow profile due to the transient temperature profile of the tumor tissue.

4. Find the oxygen concentration profile within tumor tissue due to the transient temperature profile.

1.4 Theory Used in this Study

Transport phenomena theory was used to develop electric potential profiles, transient temperature profiles, transient blood flow profiles, and transient oxygen concentration profiles.[1] The geometry studied for the electric potential profiles and the temperature profiles is shown below (Figure 1.1). This geometry studies the thermal and electrical effects of radiofrequency ablation on the tumor tissue.

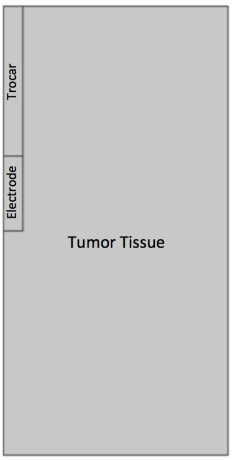

FIGURE 1.1: A 2-D axisymmetry geometry was used to develop the electric potential and temperature profiles. This geometry includes: 1) the tumor tissue within the liver; 2) the coated trocar base and tip; and 3) the radiofrequency ablation electrode.

A cylindrical geometry was used to develop the electric potential field and temperature profiles, because there is rotational symmetry in this liver tissue-electrode system. This

[1]For the values of parameters described in this section, see Section 2.

geometry includes: 1) the tumor tissue within the liver; 2) the coated trocar base and tip; and 3) the radiofrequency ablation electrode. The capillaries are excluded in this component of the study, as the capillaries have a significantly smaller radius than any other biological entity (by one thousand fold), thus having a negligible effect on the electrical and thermal profiles. This assumption is typically made in thermal biotransport studies [4, 7].

The geometry for blood flow profiles and oxygen concentration profiles is shown in Figure 1.2, which includes the capillary and the surrounding tissue.

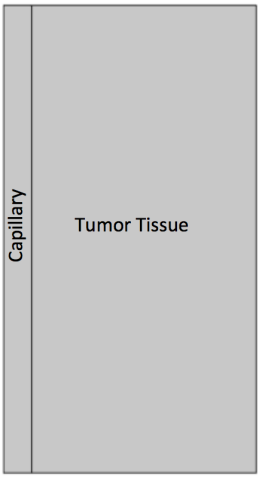

FIGURE 1.2: A 2-D axisymmetry geometry was used to develop the temperature profile. This geometry includes: 1) the capillary; and 2) the tumor tissue.

1.4.1 Electric Potential Profile Theory

1.4.1.1 Electrode Governing Equations

The electrostatic potential field for the electrode can be modeled by Poisson's equation:

$$\nabla \cdot (\sigma \nabla V_e) = -\frac{\rho_f}{\epsilon} \tag{1.1}$$

where ρ_f is the free-charge density, V_e is the electric potential of the electrode, and ϵ is the permittivity of the material. For $\rho_f = 0$, and for cylindrical coordinates with symmetry in the ϕ direction:

$$\frac{1}{r}\frac{\partial}{\partial r}(r\frac{\partial V_e}{\partial r}) + \frac{\partial}{\partial z}(\frac{\partial V_e}{\partial z}) = 0 \tag{1.2}$$

Therefore, four boundary conditions (two r and two z conditions) are required:

1. Symmetry condition in the r direction ($\frac{\partial V_e}{\partial r}|_{r=0} = 0$).

2. At the radial edge of the electrode, $V_e(r = r_{max}) = 25$ V.

3. The top z edge of the electrode is at $V_e(z = z_{max}) = 25$ V.

4. The bottom z edge of the electrode is at $V_e(z = z_{min}) = 25$ V.

1.4.1.2 Tumor Tissue Governing Equations

The electrostatic potential field of the tumor tissue can be modeled by Poisson's equation:

$$\nabla \cdot (\sigma \nabla V_{tt}) = -\frac{\rho_f}{\epsilon} \tag{1.3}$$

where ρ_f is the free-charge density, V_{tt} is the electric potential of the tumor tissue, and ϵ is the permittivity of the material. For $\rho_f = 0$, and for cylindrical coordinates with symmetry in the ϕ direction:

$$\frac{1}{r}\frac{\partial}{\partial r}(r\frac{\partial V_{tt}}{\partial r}) + \frac{\partial}{\partial z}(\frac{\partial V_{tt}}{\partial z}) = 0 \tag{1.4}$$

Therefore, four boundary conditions (two r and two z conditions) are required:

1. Symmetry condition in the r direction ($\frac{\partial V_{tt}}{\partial r}|_{r=0} = 0$).

2. The radial edge of the tissue is grounded ($V_{tt}(r = r_{max}) = 0$).

3. The top z edge of the tissue is grounded ($V_{tt}(z = z_{max}) = 0$ V).

4. The bottom z edge of the tissue is grounded ($V_{tt}(z = z_{min}) = 0$ V).

1.4.1.3 Trocar Governing Equations

The electrostatic potential field of the trocar can be modeled by Poisson's equation:

$$\nabla \cdot (\sigma \nabla V_t) = -\frac{\rho_f}{\epsilon} \tag{1.5}$$

where ρ_f is the free-charge density, V_t is the electric potential of the trocar, and ϵ is the permittivity of the material. For $\rho_f = 0$, and for cylindrical coordinates with symmetry in the ϕ direction:

$$\frac{1}{r}\frac{\partial}{\partial r}(r\frac{\partial V_t}{\partial r}) + \frac{\partial}{\partial z}(\frac{\partial V_t}{\partial z}) = 0 \tag{1.6}$$

Therefore, four boundary conditions are required:

1. Symmetry condition in the r direction ($\frac{\partial V_t}{\partial r}|_{r=0} = 0$).

2. Continuity condition on the outer r edge of the trocar.

3. The top z edge of the tissue is grounded ($V_t(z = z_{max}) = 0$ V).

4. Continuity condition on the bottom z edge of the trocar.

1.4.2 Temperature Profile Theory

1.4.2.1 Electrode Governing Equations

The governing heat equation for the electrode (constant thermal conductivity k_e, density ρ_e, and specific heat $C_{p,e}$) is:

$$\rho_e C_{p,e} \frac{\partial T_e}{\partial t} = k_e[\frac{1}{r}\frac{\partial}{\partial r}(r\frac{\partial T_e}{\partial r}) + \frac{1}{r^2}\frac{\partial}{\partial \phi}(\frac{\partial T_e}{\partial \phi}) + \frac{\partial}{\partial z}(\frac{\partial T_e}{\partial z})] + Q \tag{1.7}$$

where T_e is the temperature of the electrode, r is the radius of the electrode, ϕ is the angle coordinate of the electrode, z is the height of the electrode, and Q is the heat due to Joule heating where:

$$Q = \sigma|\nabla V|^2 \tag{1.8}$$

such that σ is the electrical conductivity. Due to symmetry, this simplifies to:

$$\rho_e C_{p,e} \frac{\partial T_e}{\partial t} = k_e[\frac{1}{r}\frac{\partial}{\partial r}(r\frac{\partial T_e}{\partial r}) + \frac{\partial}{\partial z}(\frac{\partial T_e}{\partial z})] + \sigma|\nabla V|^2 \tag{1.9}$$

Therefore, one initial condition and four boundary conditions (two r and two z conditions) are required:

1. $T_e(t = 0) = 37°\text{C}$ throughout the electrode.
2. Symmetry condition in the r direction ($\frac{\partial T_e}{\partial r}|_{r=0} = 0$).
3. Continuity condition on the outer r edge of the electrode.
4. Continuity condition on the top z edge of the electrode.
5. Continuity condition on the bottom z edge of the electrode.

1.4.2.2 Tumor Tissue Governing Equations

The governing heat equation for the tumor tissue (constant thermal conductivity k_{tt}, density ρ_{tt}, and specific heat $C_{p,tt}$) is:

$$\rho_{nt}C_{p,tt}\frac{\partial T_{tt}}{\partial t} = k[\frac{1}{r}\frac{\partial}{\partial r}(r\frac{\partial T_{tt}}{\partial r}) + \frac{1}{r^2}\frac{\partial}{\partial \phi}(\frac{\partial T_{tt}}{\partial \phi}) + \frac{\partial}{\partial z}(\frac{\partial T_{tt}}{\partial z})] + Q_m + Q + Q_b \tag{1.10}$$

where T_{tt} is the temperature of the tumor tissue, r is the radius of the tumor tissue, ϕ is the angle coordinate of the tumor tissue, z is the height of the tumor tissue, Q is the heat due to Joule heating ($Q = \sigma|\nabla V|^2$), Q_m is the metabolic heat generation, and Q_b is the blood perfusion heat generation given as:

$$\rho_b C_{p,b}\omega_b(T_b - T_{tt}) \tag{1.11}$$

where ω_b is the blood perfusion coefficient, and T_b is the blood temperature. For symmetry in the ϕ direction, this simplifies to:

$$\rho_{tt}C_{p,tt}\frac{\partial T_{tt}}{\partial t} = k[\frac{1}{r}\frac{\partial}{\partial r}(r\frac{\partial T_{tt}}{\partial r}) + \frac{\partial}{\partial z}(\frac{\partial T_{tt}}{\partial z})] + \rho_b C_{p,b}\omega_b(T_b - T_{tt}) + \sigma|\nabla V|^2 \tag{1.12}$$

Therefore, one initial condition and four boundary conditions (two r and two z conditions) are required:

1. $T_{tt}(t = 0) = 37^\circ$ C throughout the tissue.
2. Symmetry condition in the r direction ($\frac{\partial T_{tt}}{\partial r}|_{r=0} = 0$).
3. No flux condition on the outer r edge of the tumor tissue ($\frac{\partial T_{tt}}{\partial r}|_{r=r_{max}} = 0$).
4. No flux condition on the top outer z edge of the tumor tissue ($\frac{\partial T_{tt}}{\partial z}|_{z=z_{max}} = 0$).

5. No flux condition on the bottom outer z edge of the tumor tissue ($\frac{\partial T_{tt}}{\partial z}|_{z=z_{min}} = 0$).

1.4.2.3 Trocar Governing Equations

The governing heat equation for the trocar (constant thermal conductivity k_t, density ρ_t, and specific heat $C_{p,t}$) is:

$$\rho_t C_{p,t} \frac{\partial T_t}{\partial t} = k_t [\frac{1}{r} \frac{\partial}{\partial r}(r \frac{\partial T_t}{\partial r}) + \frac{1}{r^2} \frac{\partial}{\partial \phi}(\frac{\partial T_t}{\partial \phi}) + \frac{\partial}{\partial z}(\frac{\partial T_t}{\partial z})] + Q \tag{1.13}$$

where T_t is the temperature of the trocar, r is the radius of the trocar, ϕ is the angle coordinate of the trocar, z is the height of the trocar, and Q is the heat due to Joule heating where:

$$Q = \sigma |\nabla V|^2 \tag{1.14}$$

where σ is the electrical conductivity. Due to symmetry, this simplifies to:

$$\rho_t C_{p,t} \frac{\partial T_t}{\partial t} = k_t [\frac{1}{r} \frac{\partial}{\partial r}(r \frac{\partial T_t}{\partial r}) + \frac{\partial}{\partial z}(\frac{\partial T_t}{\partial z})] + \sigma |\nabla V|^2 \tag{1.15}$$

Therefore, one initial condition and four boundary conditions (two r and two z conditions) are required:

1. $T_t(t = 0) = 37^\circ$ C throughout the trocar.

2. Symmetry condition in the r direction ($\frac{\partial T_e}{\partial r}|_{r=0} = 0$).

3. Continuity condition on the outer r edge of the trocar.

4. No flux condition on the top outer z edge of the trocar ($\frac{\partial T_t}{\partial z}|_{z=z_{max}} = 0$).

5. Continuity condition on the bottom outer z edge of the trocar.

1.4.3 Blood Flow Profile Theory

1.4.3.1 Capillary Governing Equations

Blood flow inside the capillary is governed by both the continuity and the Navier-Stokes equations (for constant density, and flow only in the z direction):

$$\frac{\partial u_z}{\partial z} = 0 \tag{1.16}$$

$$\rho_b(\frac{\partial u_z}{\partial t} + u_z\frac{\partial u_z}{\partial z}) = -\frac{\partial p}{\partial z} + \mu[\frac{1}{r}\frac{\partial}{\partial r}(r\frac{\partial u_z}{\partial r} + \frac{\partial^2 u_z}{\partial z^2}] \tag{1.17}$$

where u_z is the velocity in the z direction, μ is the blood viscosity, and r is a function of average temperature of the tumor such that:

$$r = r_0\sqrt{e^{b(T-T_0)}} \tag{1.18}$$

where r_0 is the known initial capillary radius, and T_0 is the known initial capillary temperature. From the governing equations, one initial velocity condition, one pressure boundary condition, and four velocity boundary conditions (two r and two z conditions) are required:

1. Initial u_z is known and calculated from the pressure drop (which is specified throughout the tube).

2. Inlet pressure at bottom of capillary ($p(z = z_{min})$) is specified.

3. No slip condition at the wall ($u_z(r = r_{max}) = 0$).

4. Symmetry condition ($\frac{\partial u_z}{\partial r}|_{r=0} = 0$).

5. No momentum flux at bottom of wall ($\frac{\partial u_z}{\partial z}|_{z=z_{min}} = 0$).

6. No momentum flux at top of wall ($\frac{\partial u_z}{\partial z}|_{z=z_{max}} = 0$).

It is assumed there is no blood flow velocity profile in the tumor tissue.

1.4.4 Oxygen Transport Theory

Oxygen transport in biological systems are typically modeled in terms of oxygen partial pressures (P_{O_2}).

1.4.4.1 Capillary Governing Equations

Oxygen diffusion inside the capillary is governed by:

$$\frac{\partial P_{O_2}}{\partial t} + u_z \frac{\partial P_{O_2}}{\partial r} = D[\frac{1}{r}\frac{\partial}{\partial r}(r\frac{\partial P_{O_2}}{\partial r}) + \frac{\partial^2 P_{O_2}}{\partial z^2}] - \frac{M}{a} \tag{1.19}$$

where D is the diffusivity constant, M is the rate of metabolism, and a is the oxygen solubility. This requires five conditions (an initial condition, and four boundary conditions (two r and two z conditions)):

1. Initial oxygen partial pressure is known ($P_{O_2}(t = 0) = P_{O_2,i}$ at inlet of capillary tube, 0 elsewhere).

2. Symmetry condition ($\frac{\partial P_{O_2}}{\partial r}|_{r=0} = 0$).

3. No flux at bottom wall in z direction ($\frac{\partial P_{O_2}}{\partial z}|_{z=z_{min}} = 0$).

4. No flux at top wall in z direction ($\frac{\partial P_{O_2}}{\partial z}|_{z=z_{max}} = 0$).

5. Continuity condition at far wall in r direction.

1.4.4.2 Tumor Tissue

Oxygen diffusion inside the tumor tissue is governed by:

$$\frac{\partial P_{O_2}}{\partial t} + u_z \frac{\partial P_{O_2}}{\partial r} = D[\frac{1}{r}\frac{\partial}{\partial r}(r\frac{\partial P_{O_2}}{\partial r}) + \frac{\partial^2 P_{O_2}}{\partial z^2}] - \frac{M}{a} \tag{1.20}$$

where D is the diffusivity constant, M is the rate of metabolism, and a is the oxygen solubility. This requires five conditions (an initial condition, and four boundary conditions (two r and two z conditions)):

1. Initial oxygen partial pressure is known ($P_{O_2}(t = 0) = 0$ throughout tumor tissue).

2. Continuity condition at near wall in r direction.

3. No flux at bottom wall in z direction ($\frac{\partial P_{O_2}}{\partial z}|_{z=z_{min}} = 0$).

4. No flux at top wall in z direction ($\frac{\partial P_{O_2}}{\partial z}|_{z=z_{max}} = 0$).

5. No flux at far wall in r direction ($\frac{\partial P_{O_2}}{\partial r}|_{r=r_{max}} = 0$).

Procedure

To mathematically describe the effects of radiofrequency ablation on blood flow and oxygen transport within both tumor tissue and normal tissue, COMSOL Multiphysics was used. The following general steps were taken:

1. Develop the electric potential profile.
2. Develop the transient temperature profile due to radiofrequency ablation.
3. Determine the blood flow profile due to the transient temperature profile.
4. Find the oxygen concentration profile within both normal tissue and tumor tissue.

The method to develop the electric potential and temperature profiles due to radiofrequency ablation are shown in the following section.

2.1 Electric Potential and Temperature Profile Methodology

To develop the electric potential and temperature profiles, COMSOL Multiphysics was used. First, the "Heat Transfer in Solids" and "Electric Currents" physics options were selected, using a transient analysis. Next, it was necessary to build the geometry of this system.

A 2-D axisymmetry geometry was used to develop the temperature and electric potential profiles. This geometry includes: 1) the tumor tissue within the liver; 2) the coated trocar base and tip; and 3) the radiofrequency ablation electrode. The capillaries are excluded in this component of the study, as the capillaries have a significantly smaller radius than any other biological entity (by one thousand fold), thus having a negligible effect on the electrical and thermal profiles. This assumption is typically made in thermal biotransport studies [4, 7]. The geometry of this study is shown in Figure 2.1.

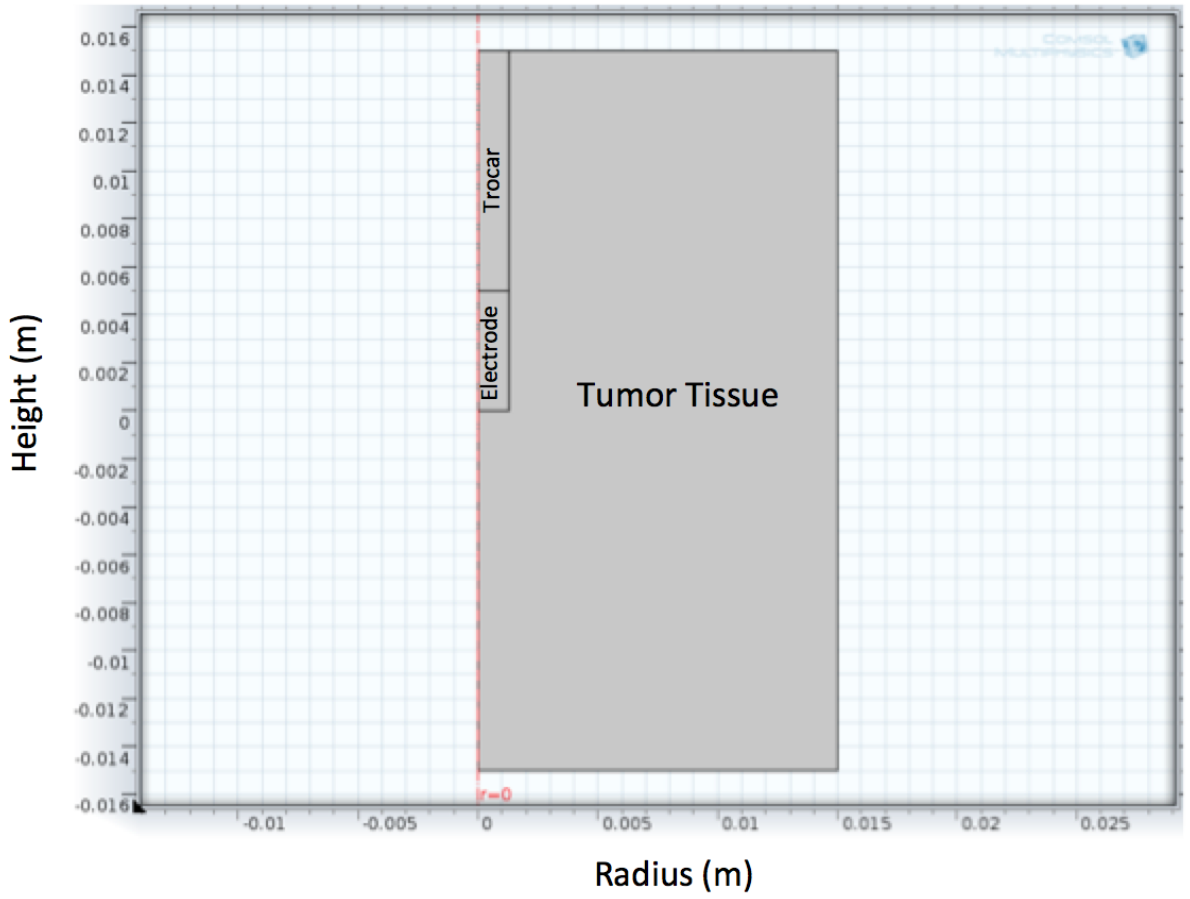

FIGURE 2.1: A 2-D axisymmetry geometry was used to develop the temperature profile. This geometry includes: 1) the normal liver tissue; 2) the tumor tissue within the liver; 3) the coated trocar base and tip; and 4) the radiofrequency ablation electrode.

The lengths of each component which were used within the system are shown in Table 2.1.

TABLE 2.1: Length of Components Within Biological System

Component	Length (mm)	Reference
Electrode Radius	1.3	[8]
Electrode Height	5.0	[8]
Trocar Radius	1.3	[8]
Trocar Height	10.0	[8]
Tumor Tissue Radius	15	[8]
Tumor Tissue Height	30	[8]

The material properties of each component which were used within the system are shown below (Table 2.2).

TABLE 2.2: Material Properties of Components Within Biological System

Property	Electrode	Trocar	Tumor Tissue	References
k (W/m/k)	71	0.26	0.48	[7, 8]
ρ (kg/m^3)	21,500	70	1,050	[7, 8]
C_p (J/kg/K)	132	1,045	3,770	[7, 8]
σ (S/m)	4×10^6	1×10^{-4}	0.222	[7, 8]
ϵ	0.9	0.9	0.9	[7, 8]

Next, it was necessary to declare the initial conditions and boundary conditions, as well as generation terms, for each component of the system for the "Heat Transfer in Solids" physics. Therefore, the following options were selected:

1. Axial symmetry for each component.

2. Thermal insulation for the outer boundary of the system.

3. Heat transfer in solids for the trocar and the electrode.

4. Initial value of 310.15 K for each component in the system.

5. Heat source as a function of total power dissipation density.

6. Biological tissue for the tumor tissue, with bioheat characteristics of:

    - $\rho_b = 1,100$ kg/m^3
    - $C_{p,b} = 3,300$ J/kg/K
    - $\omega = 0.01$ 1/s
    - $T_b = 310.15$ K
    - $Q_m = 65,400$ W/m^3

Conditions were also established for the "Electric Currents" physics, such that:

1. Axial symmetry for each component.

2. Current conservation for each component with their respective materials.

3. Grounding at the outer boundaries of the system.

4. 25 V for the outer boundaries of the electrode geometry.

The "finer" element size mesh was selected, and the study was run at 0.1 s intervals for 60 seconds.

For the next portion of the study, the average temperature of the tissue was necessary. Therefore, an integration operator was established, and was implemented on the tumor tissue to find the average tumor tissue temperature by:

$$T_{avg} = \frac{\int \int_S T_{tt} dS}{A_{tt}} \tag{2.1}$$

where A_{tt} is the tumor tissue surface area. This data was subsequently exported to a ".csv" file.

2.2 Blood Flow and Oxygen Transport Profile Methodology

To develop the blood flow and oxygen transport profiles, COMSOL Multiphysics was used. First, the "Non-Isothermal Flow", "Transport of Diluted Species", and "Deformed Geometry" physics options were selected, using a transient analysis. Next, it was necessary to build the geometry of this system.

A 2-D axisymmetry geometry was used to develop the blood flow and oxygen profiles. This geometry includes: 1) the capillary; and 2) the surrounding tumor tissue. The geometry of this study is shown in Figure 2.1. A smaller tumor tissue system was analyzed, as the radius of a capillary is one thousand-fold smaller than the radius of the tissue.

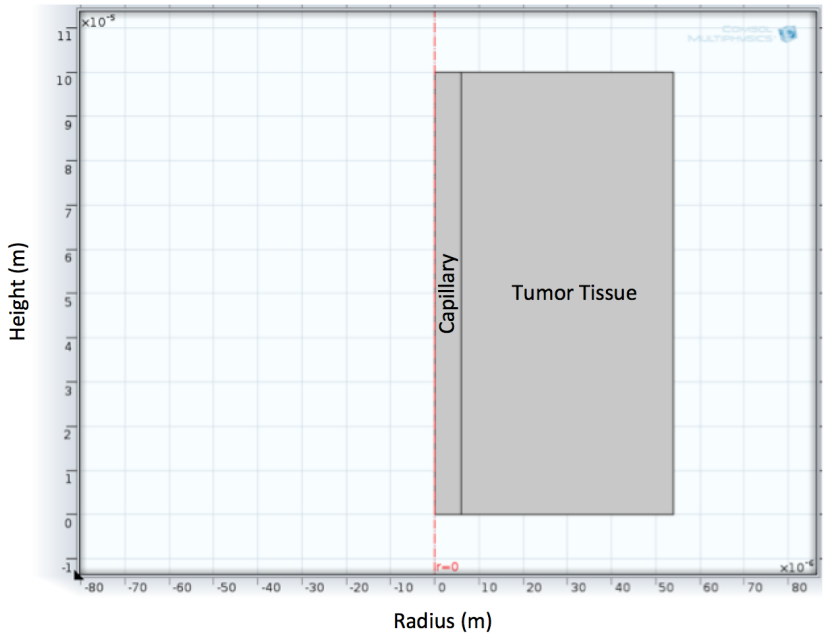

FIGURE 2.2: A 2-D axisymmetry geometry was used to develop the blood flow and oxygen profiles. This geometry includes: 1) the capillary; and 2) the surrounding tumor tissue.

The lengths of each component which were used within the system are shown in Table 2.3. The dynamic viscosity (μ) for the capillary was 0.0044 Pa·s, and the diffusivity constant for both the capillary and the surrounding tumor tissue was 1.5×10^{-9} m^2/s.

TABLE 2.3: Length of Components Within Biological System

Component	Length (μm)	Reference
Capillary Radius	6	[8]
Capillary Height	100	[8]
Tumor Radius	54	[8]
Tumor Height	100	[8]

The geometry changes over time, making it necessary to define the displacement and velocity of the geometry. Therefore, it was necessary to open the ".csv" file saved from the previous study, and to calculate the radius of the capillary as a function of time by:

$$r = r_0\sqrt{e^{b(T-T_0)}} \tag{2.2}$$

where r_0 is the original capillary radius defined in Table 2.3, and T_0 is normal human body temperature (310.15 K). Next, it was necessary to find the rate of change of the radius (i.e. $\frac{dr}{dt}$), by calculating $\frac{dr}{dt} \approx \frac{\Delta r}{\Delta t}$. The rate of change of the radius as a function of time was subsequently exported into a ".txt" file. Finally, an interpolation velocity function (labeled as "vel(t)") was inserted, using the ".txt" file as data for this operation. Next, it was necessary to declare conditions for each component of the system for the "Deformed Geometry" physics. Therefore, the following options were selected:

1. Free deformation for each component.

2. Prescribed r and z velocities of 0 m/s for the outer boundaries of the system.

3. Prescribed r velocity of "vel(t)" for the outer capillary wall.

Subsequently, it was necessary to declare conditions for the capillary system for the "Non-Isothermal Flow" physics. Therefore, the following options were selected:

1. An inlet pressure of 2307 Pa.

2. An outlet pressure of 1160 Pa.

3. A no slip condition on the outer wall.

Next, it was necessary to declare conditions for the each component within the system for the "Transport of Diluted Species" physics. Therefore, the following options were selected:

1. No flux on the outer tissue boundaries.

2. A reaction of -1.1 mm Hg/s for both boundaries.

3. A concentration of 50 mm Hg at the inlet of the capillary.

4. An outflow at the outlet of the capillary.

Finally, a "normal" element size mesh was selected, and the study was run at 0.1 s intervals for 60 seconds.

Results and Discussion

In this study, a mathematical model was successfully developed via COMSOL Multiphysics to describe the effects of radiofrequency ablation on blood flow and oxygen transport within tumor tissue. To determine the effects of radiofrequency ablation on blood flow and oxygen transport within tumor tissue, it was first necessary to determine the temperature and electric potential profiles.

3.1 Temperature and Electric Potential Profiles

To determine the contribution of Joule heating on the temperature profiles, the electric potential profile was first examined (Figure 3.1). The electric potential field was independent of time, which was expected from the governing equations. Specifically, the governing equation within each component of the system is given as:

$$\frac{1}{r}\frac{\partial}{\partial r}(r\frac{\partial V}{\partial r}) + \frac{\partial}{\partial z}(\frac{\partial V}{\partial z}) = 0 \tag{3.1}$$

This electric potential profile has no time dependence, making it a steady-state study on the electric potential field. To confirm this result, a steady-state analysis was performed on COMSOL on the electric potential field, and the same electric potential profile was

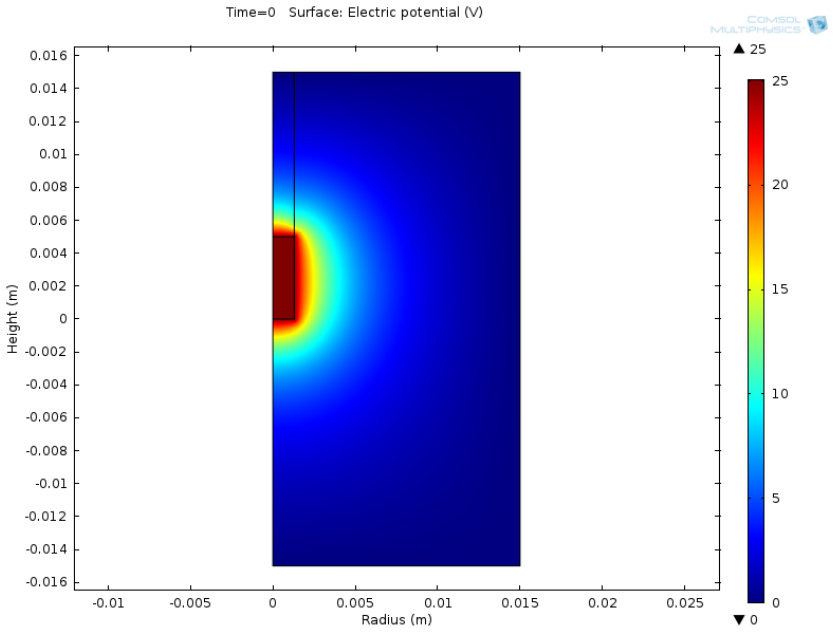

FIGURE 3.1: The electric potential profile provides insight into Joule heating. The electric potential field was indepedent of voltage, as expected.

generated. This profile contains gradients, which demonstrates a Joule heating effect exists. The resulting temperature profile after 60 seconds of radiofrequency ablation via Joule heating is shown below (Figure 3.2).

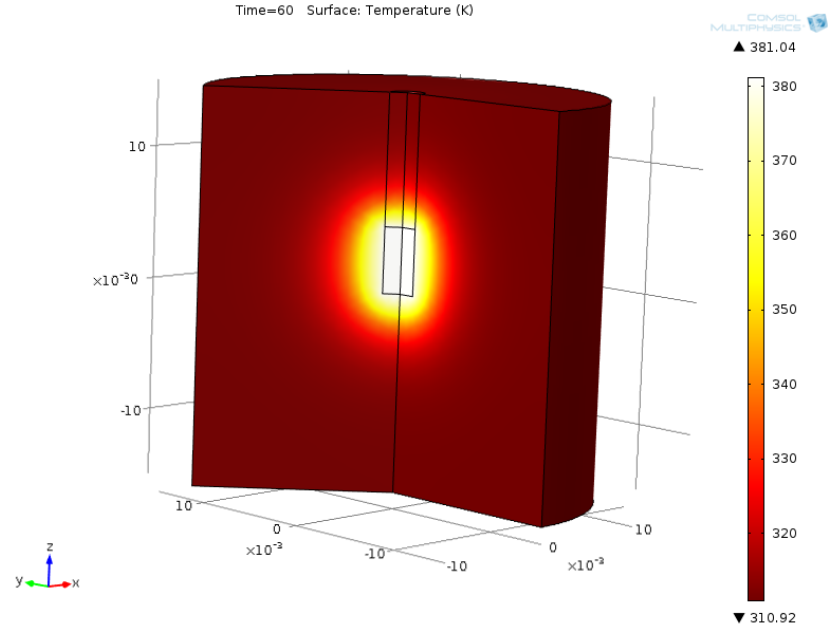

FIGURE 3.2: The temperature profile after 60 seconds of radiofrequency ablation.

As shown in the temperature profile, the maximum temperature of the electrode-tissue system reaches 381 K. The transient temperature profile within the tissue (at a height of $z = 0$) is shown in Figure 3.3.

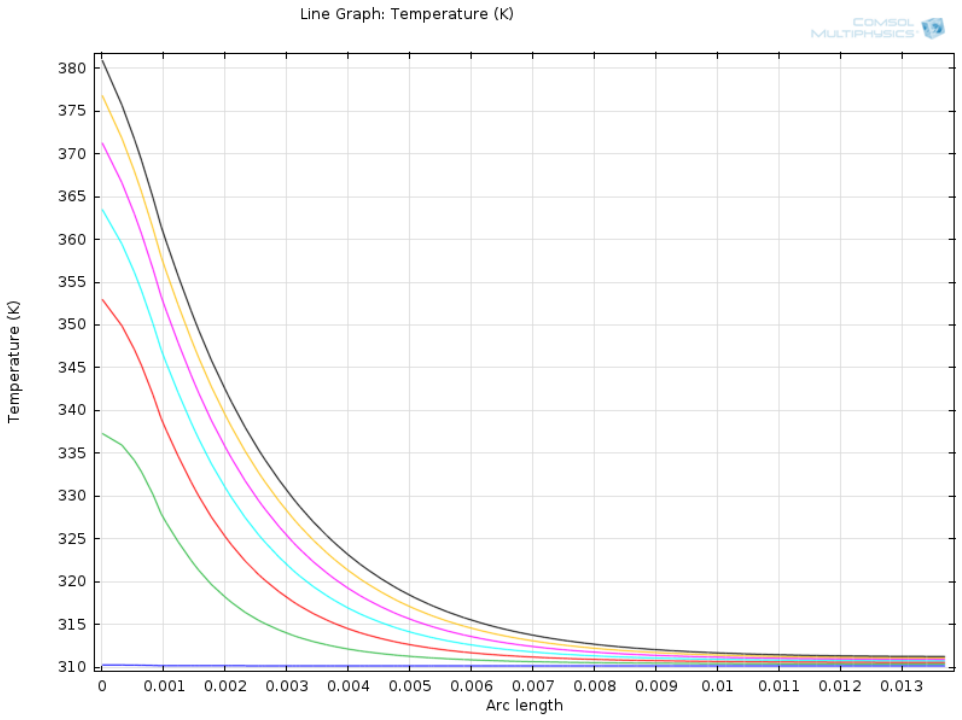

FIGURE 3.3: The transient temperature profile of the tumor tissue was analyzed. As time increased, the temperature within the tissue would increase. The tissue temperature reaches a maximum of 381 K.

As shown in Figure 3.3, as time increased, the temperature within the tissue would also increase as expected. The tissue temperature reaches a maximum of 381 K after 60 seconds.

To develop the blood flow and oxygen transport profiles, it was necessary to find the tissue average temperature as a function of time. This relationship is shown in Figure 3.4. As expected, as time increases, the average temperature of the tissue increases. The maximum average temperature of the tissue during the duration of radiofrequency

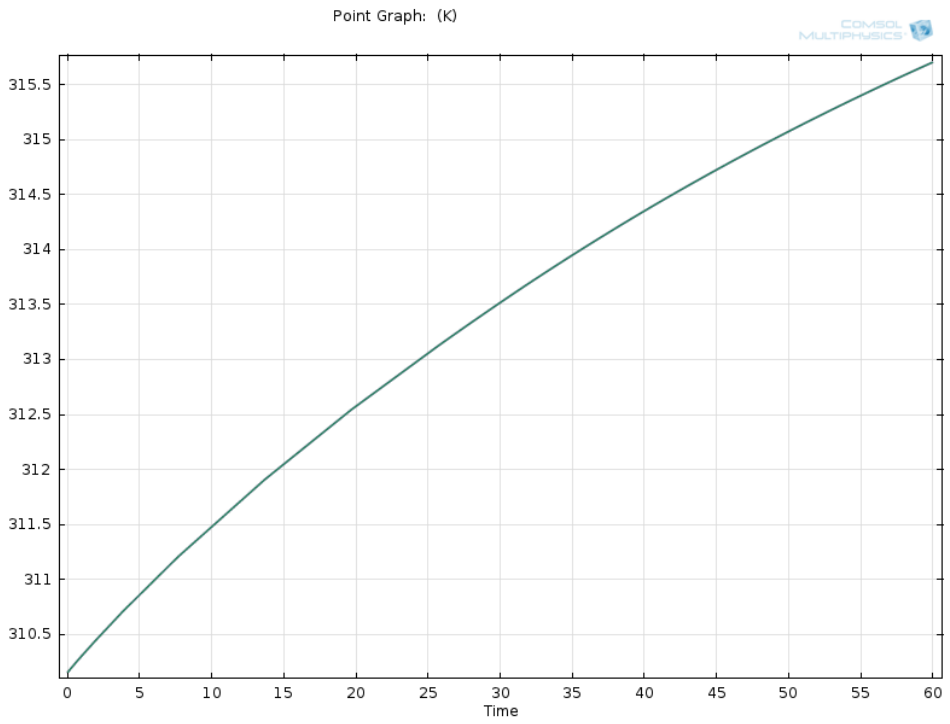

FIGURE 3.4: The average tissue temperature profile was analyzed to determine the changes in blood flow and oxygen transport profiles in capillaries. As time increased, the average temperature within the tissue would increase.

ablation was 316 K. The average temperature as a function of time was used to determine the radius of the capillary over time, which is discussed in the following section.

3.2 Blood Flow and Oxygen Transport Profiles

The main focus of this study was the effects of radiofrequency ablation on blood flow and oxygen transport. The radius of a capillary is affected by the average temperature of a tumor, where:

$$r = r_0\sqrt{e^{b(T-T_0)}} \tag{3.2}$$

Therefore, since the average temperature of the tissue increased over the duration of radiofrequency ablation, it was expected that the radius of the capillary would increase.

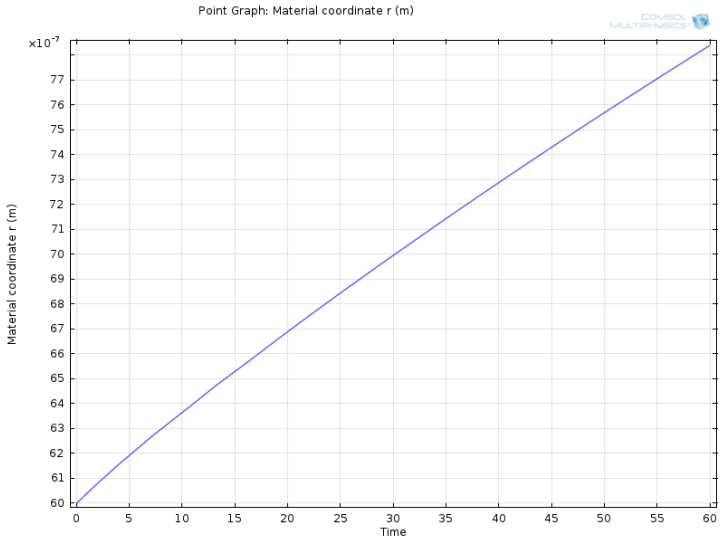

FIGURE 3.5: Since the average temperature of the tissue increased over the duration of radiofrequency ablation, the radius of the capillary also increased. The radius of a capillary increased by 30% after 60 seconds of ablation.

In Figure 3.5, it is evident that the radius of a capillary increases by 30% after 60 seconds of radiofrequency ablation. The resulting effects on the blood flow and oxygen transport profiles are discussed below.

The transient blood flow velocity was evaluated at the center of the capillary (Figure 3.6).

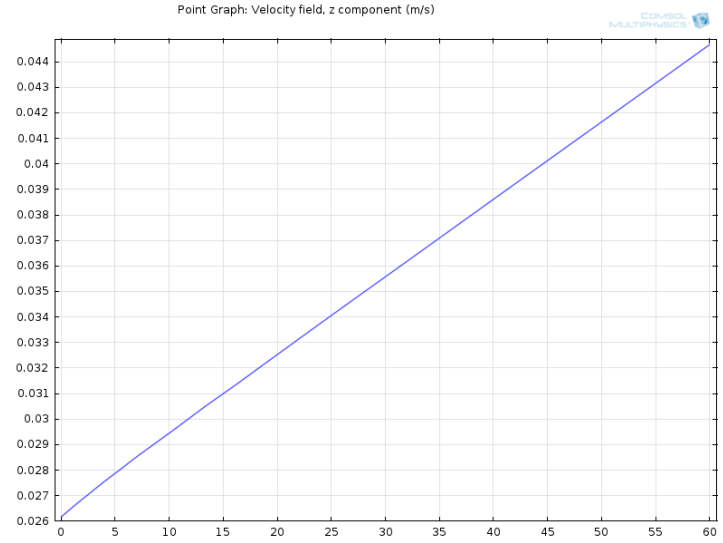

FIGURE 3.6: Since the average temperature of the tissue increased over the duration of radiofrequency ablation, the radius of the capillary also increased. As a result, the blood flow velocity increased from 0.026 m/s to 0.045 m/s.

As shown in Figure 3.6, the blood flow velocity increased from 0.026 m/s to 0.046 m/s. This was a result of the increased radius of the capillary with a maintained pressure drop. If the radius of the capillary did not change, the maximum blood flow velocity would have stayed at 0.026 m/s. This shows that radiofrequency ablation can potentially be coupled with chemotherapy to enhance the efficacy of delivering pharmacological agents. The velocity profile after 60 seconds of radiofrequency ablation is shown below (Figure 3.7).

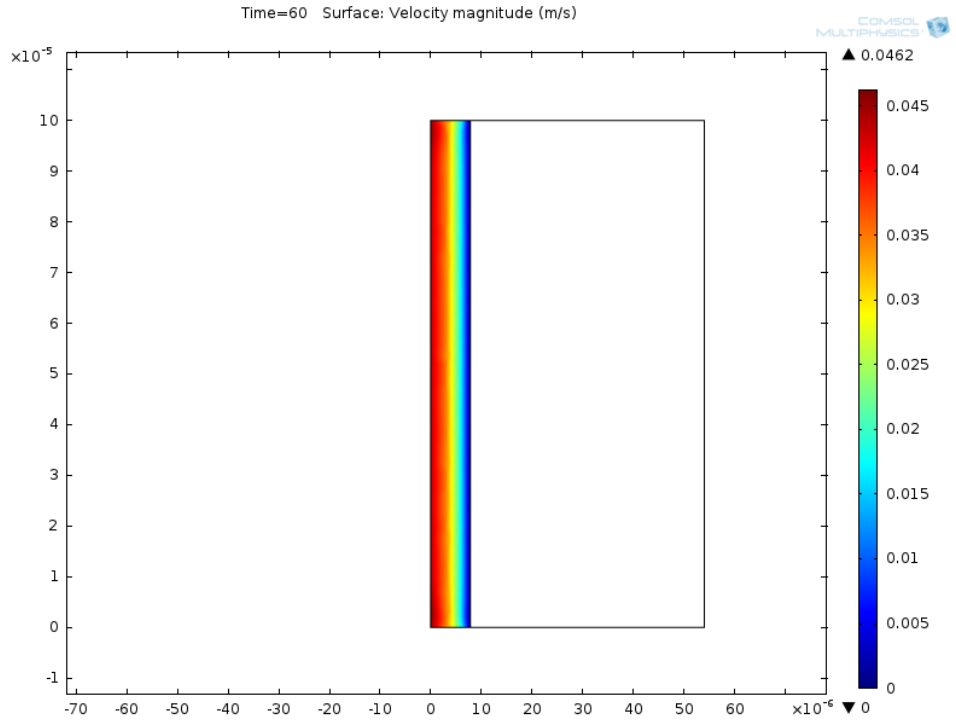

FIGURE 3.7: The capillary blood flow profile at 60 seconds is shown.

As expected, the maximum blood flow velocity is at the center of the capillary. Furthermore, at the radial edges of the capillary, the no slip condition was applied, where the blood flow velocity is zero. There was no blood flow in the tumor tissue where capillaries did not exist.

Next, the effects of radiofrequency ablation on oxygen transport in the capillaries were considered. The oxygen transport within the capillary and the surrounding tumor tissue

with and without radiofrequency ablation is shown in Figure 3.8.

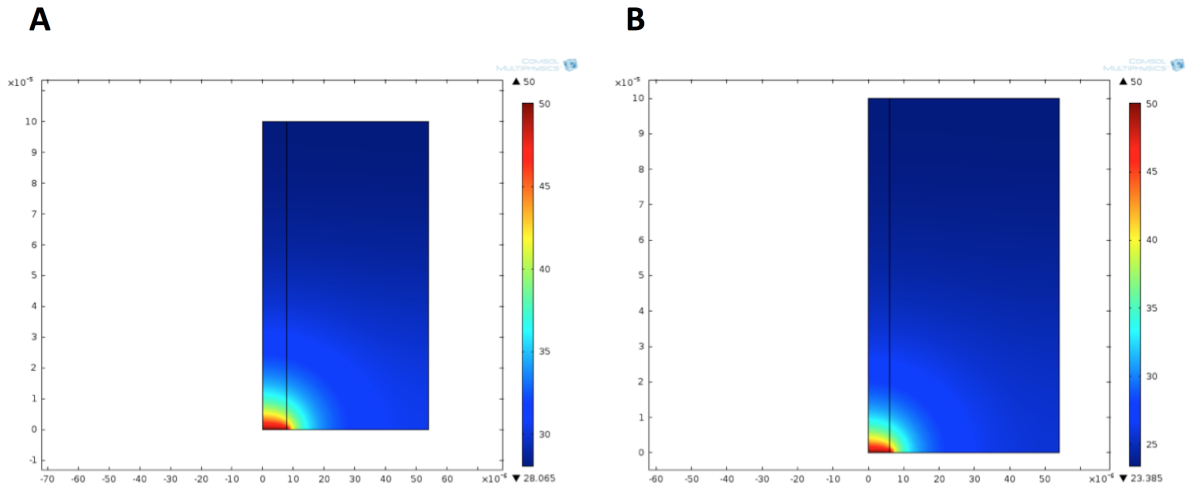

FIGURE 3.8: Oxygen transport within the capillary and the surrounding tumor tissue with (A) and without (B) radiofrequency ablation. There is greater overall oxygen transport when radiofrequency ablation is applied.

As shown in Figure 3.8, there is greater overall oxygen transport when radiofrequency ablation is applied. The minimum partial pressure of oxygen of the system was 28 mm Hg with ablation, compared to 23 mm Hg without ablation. This also demonstrates the beneficial microvasculature effects of radiofrequency ablation.

Conclusions

A mathematical model was successfully developed via COMSOL Multiphysics to describe the effects of radiofrequency ablation on blood flow and oxygen transport within tumor tissue. It was determined that the application of radiofrequency ablation on cancerous liver tissue for 60 seconds increases the average temperature of the entire tumor tissue from 37°C to 43°C. The hyperthermic effects of radiofrequency ablation subsequently resulted in an increase of capillary blood vessel radius by 30%, an increase in blood flow velocity by 70%, and an increase in overall oxygenation. This study shows that radiofrequency ablation can potentially be coupled with chemotherapy to enhance the efficacy of delivering pharmacological agents. Future work includes examining the effects of radiofrequency ablation on drug delivery to cancerous liver tissue.

Bibliography

[1] MUSC Health. Liver tumors. URL http://www.muschealth.com/gs/healthtopic.aspx?action=showpage&pageid=P00688.

[2] Standford Medicine. Benign versus malignant. URL http://cancer.stanford.edu/endocrine/benignvmalignant.html.

[3] American Cancer Society. Cancer facts and figures 2014. *American Cancer Society*, 2014.

[4] S. Tungjitkusolmun, Eung Je Woo, Hong Cao, Jang-Zern Tsai, V.R. Vorperian, and J.G. Webster. Finite element analyses of uniform current density electrodes for radio-frequency cardiac ablation. *Biomedical Engineering, IEEE Transactions on*, 47(1): 32–40, Jan 2000. ISSN 0018-9294. doi: 10.1109/10.817617.

[5] B. Endrich, F. Hammersen, and K. Messmer. Hyperthermia-induced changes in tumor microcirculation. *Recent results in cancer research. Fortschritte der Krebsforschung. Progrès dans les recherches sur le cancer*, 107:44–59, 1988. ISSN 0080-0015. URL http://www.ncbi.nlm.nih.gov/pubmed/3375562.

[6] A. Shakil, J. L. Osborn, and C. W. Song. Changes in oxygenation status and blood flow in a rat tumor model by mild temperature hyperthermia. *International journal of*

radiation oncology, biology, physics, 43(4):859–865, Mar 1999. ISSN 0360-3016. URL http://www.ncbi.nlm.nih.gov/pubmed/10098442.

[7] Ying He, Minoru Shirazaki, Hao Liu, Ryutaro Himeno, and Zhigang Sun. A numerical coupling model to analyze the blood flow, temperature, and oxygen transport in human breast tumor under laser irradiation. *Computers in biology and medicine*, 36 (12):1336–1350, Dec 2006. ISSN 0010-4825. doi: 10.1016/j.compbiomed.2005.08.004. URL http://www.ncbi.nlm.nih.gov/pubmed/16263105.

[8] Datta A and Rakesh V. *An Introduction to Modeling of Transport Processes: Applications to Biomedical Systems*. Cambridge University Press, 2010.